

The Real Gauge Singlet Scalar Extension of Standard Model: A Possible Candidate of Cold Dark Matter

Anirban Biswas ¹, Debasish Majumdar ²

*Astroparticle Physics and Cosmology Division,
Saha Institute of Nuclear Physics,
1/AF Bidhannagar, Kolkata 700064, India*

ABSTRACT

We consider a simplest extension of Standard Model in which a real SM gauge singlet scalar with an additional discrete symmetry Z_2 is introduced to SM. This additional scalar can be a viable candidate of cold dark matter since the stability of S is achieved by the application of Z_2 symmetry on S . Considering S as a possible candidate of cold dark matter we have solved Boltzmann's equation to find the freeze out temperature and relic density of S for Higgs mass 120 GeV in the scalar mass range 5 GeV to 1 TeV. As $HHSS$ coupling δ_2 appearing in Lagrangian depends upon the value of scalar mass m_S and Higgs mass m_h , we have constrained the $m_S - \delta_2$ parameter space by using the WMAP limit on the relic density of dark matter in the universe and the results of recent ongoing dark matter direct search experiments namely CDMS-II, CoGeNT, DAMA, EDELWEISS-II, XENON-10, XENON-100. From such analysis we find two distinct mass regions (a lower and higher mass domain) for such a dark matter candidate that satisfy both the WMAP limit and the experimental results considered here. We have estimated the possible differential direct detection rates and annual variation of total detection rates for this scalar dark matter candidate S for two detector materials namely Ge, Xe. Finally we have calculated the γ -ray flux from the galactic centre due to annihilation of two 130 GeV scalar dark matter into two monoenergetic γ -rays.

Pacs: 95.35.+d, 98.80.Cq

Dark Matter, Beyond SM

¹email: anirban.biswas@saha.ac.in

²email: debasish.majumdar@saha.ac.in

1 Introduction

In recent years, one of the most important areas of modern cosmology is to investigate the existence and nature of dark matter in the universe. The observations by Wilkinson Microwave Anisotropy Probe (WMAP) [1] for studying the fluctuations in cosmic microwave background radiation reveal that the universe consists of 27% matter and the rest 73% is an unknown energy known as Dark Energy. Out of this 27%, only about 4% accounts for the ordinary matter like leptons and baryons, gas, stars and galaxies etc. The rest about 23% matter is completely unknown. Moreover there are several cosmological observations like rotation curves of spiral galaxies, the gravitational micro-lensing, observations on Virgo [2] and Coma clusters [3], bullet clusters [4], etc. which provide indications of the existence of huge amount of non-luminous matter or dark matter (DM) in the universe.

Nature and identity of the constituents of dark matter are mostly unknown. However, evidences suggest that the dark matter candidates are mostly stable, non-baryonic, massive, non-relativistic particles having negligible or very weak interactions with other particles. These types of dark matter are often termed as cold dark matter (CDM) or weakly interacting massive particles (WIMP). In the early universe, these particles would have been present in large numbers in thermal equilibrium. As the universe expands and cools down their density decreases resulting in decrease in their interaction/annihilation rates. When the expansion rate of the universe becomes larger than the annihilation rate of the WIMPs, they get decoupled from the universe. Thus they “freeze out” from the other contents of the universe and remain as relics. The temperature at which this phenomenon occurs is known as “freeze out” temperature and its density is called “relic density”. After freeze out, the relic density of WIMP is only affected by the expansion of the universe. Since Standard Model (SM) of particle physics cannot provide any viable candidate for cold dark matter, one has to consider theories beyond SM in order to explain the dark matter candidates (namely WIMP).

In this paper we have considered the simplest possible renormalisable extension of SM by adding a real gauge singlet scalar S . We impose a discrete symmetry Z_2 on S and due to this symmetry the additional scalar S is stable and can be a viable candidate for cold dark matter. This model was first proposed by V. Silveira and A. Zee [5]. Thereafter a number of authors have explored its phenomenology [6]. The relevance of the scalar singlet as a plausible candidate for dark matter is very elaborately described in Ref. [7] (and references therein). Investigating the relic density of a scalar dark matter by constraining the unknown parameters from direct detection experiments are addressed by previous authors. In Ref. [8], the relic density is investigated for scalar singlet by constraining dark matter mass and direct detection rates from DAMA [9] results. Similar analysis including the CoGeNT [10] results and CDMS II [11] results

are also addressed in Ref. [12]. The analysis of scalar singlet dark matter scenario for XENON 100 [13] direct detection experiment results are also given in this reference. The scalar singlet dark matter with CoGeNT results are also discussed by Fitzpatrick et al [14]. The interpretation of Fermi-Lat results [15] with scalar singlet dark matter is discussed in Ref. [16].

In the present work we estimate the freeze out temperature and relic density of the dark matter candidate S by solving Boltzmann's equation. Then we constrain the parameter δ_2 ³ by using WMAP limit on relic density of dark matter and the results of recent dark matter direct detection experiments like CDMS-II [11, 17], XENON-10 [18], XENON-100 [13], CoGeNT [10, 19], EDELWEISS-II [20] and DAMA [9]. In CDMS and CoGeNT experiments the target material is Ge and in XENON experiments the target materials is Xe.

The constrained parameters thus obtained are then used to calculate the differential direct detection rates and the annual variation of total detection rates of the scalar dark matter candidate S for two detector materials namely Ge, Xe. Therefore we have calculated the γ -ray flux due to 130 GeV scalar dark matter for the annihilation channel $SS \rightarrow \gamma\gamma$ from the galactic centre.

The paper is organised as follows. In Section 2 we give a brief description of the scalar singlet model. Section 3 describes the formalism for computing relic abundance of a particular particle candidate. The results of the relic density calculations are given in Section 4. The model parameter δ_2 is constrained using the WMAP relic density data and the results obtained from various dark matter direct detection experiments. This is described in Section 5. The formalism for the calculation of direct detection rates and the annual variations of these rates is described in Section 6. With the constrained model parameter, δ_2 as obtained in Section 5, the direct detection rates and their annual variations of total detection rates are calculated for this scalar dark matter candidate for some reference detector materials namely Ge, Xe. The calculational procedure and the results are described in Section 7. In section 8 we have calculated the γ -ray flux from galactic centre due to annihilation of dark matter present in the galactic halo. Finally in Section 9, we give a summary and conclusion.

2 The Model

In the present work we consider a simplest extension of Standard Model where a real singlet scalar is added to the scalar sector of SM and explore the possibility that it can be a candidate for cold dark matter. The most general form of the potential appearing in the Lagrangian density

³only parameter in this model which appears in both the expressions of scattering and annihilation cross section of S and which depends on the masses of scalar S and Higgs h

for such a scalar fields is

$$V(H, S) = \frac{m^2}{2} H^\dagger H + \frac{\lambda}{4} (H^\dagger H)^2 + \frac{\delta_1}{2} H^\dagger H S + \frac{\delta_2}{2} H^\dagger H S^2 + \left(\frac{\delta_1 m^2}{2\lambda} \right) S + \frac{k_2}{2} S^2 + \frac{k_3}{3} S^3 + \frac{k_4}{4} S^4 \quad (1)$$

and the Lagrangian of this model is given by

$$\mathcal{L} = \mathcal{L}_{\text{SM}} + \frac{1}{2} \partial_\mu S \partial^\mu S - \frac{\delta_1}{2} H^\dagger H S - \frac{\delta_2}{2} H^\dagger H S^2 - \left(\frac{\delta_1 m^2}{2\lambda} \right) S - \frac{k_2}{2} S^2 - \frac{k_3}{3} S^3 - \frac{k_4}{4} S^4 \quad (2)$$

Where \mathcal{L}_{SM} is the Standard Model (SM) Lagrangian, H is the SM Higgs doublet and S is the real gauge $(\text{SU}(2)_L \times \text{U}(1)_Y)$ singlet scalar. The stability of S will be achieved by imposing a Z_2 symmetry ($S \rightarrow -S$, $\mathcal{L} \rightarrow \mathcal{L}$) over S . Therefore, under this symmetry the coefficients of odd powers of S are zero (k_3 and δ_1 in Eq. (2)). After spontaneous symmetry breaking masses of the Scalar field S and physical Higgs h are

$$m_S^2 = k_2 + \delta_2 V^2/2, \quad (3)$$

$$m_h^2 = -m^2 = \lambda V^2/2, \quad (4)$$

V is the VEV of Higgs ($V = 246$ GeV). In the present work we have taken the mass m_S of the scalar particle S in the range 5 GeV - 1 TeV. Depending on its mass the dark matter candidate S annihilates into fermion pairs, gauge boson pairs and Higgs pairs.

3 Formalism for Calculation of Relic Abundance

In order to calculate the relic abundance of the scalar particle S we have solved numerically the Boltzmann's equation which is given by

$$\frac{dn}{dt} + 3Hn = -\langle \sigma v \rangle (n^2 - n_{\text{eq}}^2), \quad (5)$$

where n is the number density of the scalar particle S and n_{eq} is the value of n when S was in equilibrium (when temperature $T > T_f$, T_f being the freeze out temperature of S), H denotes the Hubble parameter, $\langle \sigma v \rangle$ is the thermal average of the product of annihilation cross section and the relative velocity of the two annihilating particles (in this case the scalar singlet S). It is useful to define two dimensionless quantities, $Y = n/s$ [21] and $x = m/T$. Where s is the total

entropy density of the universe, T being the photon temperature. From the standard Friedmann-Robertson-Walker cosmology, the Hubble parameter $H = \sqrt{\frac{8}{3}\pi G\rho}$ and G is the gravitational constant. The total energy density (ρ) and the total entropy density (s) of the universe are given by [21]

$$\rho = g_{eff}(T) \frac{\pi^2}{30} T^4 \quad (6)$$

$$\text{and } s = h_{eff}(T) \frac{2\pi^2}{45} T^3 . \quad (7)$$

In Eqs.(6) and (7) g_{eff} , h_{eff} are the effective degrees of freedom for the energy and entropy densities. Substituting Eqs. (6), (7) and the expression of H into Eq. (5), we arrive at the equation for the evolution of Y as

$$\frac{dY}{dx} = - \left(\frac{45}{\pi} G \right)^{-1/2} \frac{g_*^{1/2} m}{x^2} \langle \sigma v \rangle (Y^2 - Y_{eq}^2) , \quad (8)$$

where $g_*^{1/2}$ is defined as [21]

$$g_*^{1/2} = \frac{h_{eff}}{g_{eff}^{1/2}} \left(1 + \frac{1}{3} \frac{T}{h_{eff}} \frac{dh_{eff}}{dT} \right) . \quad (9)$$

Y_{eq} is the value of Y when $n = n_{eq}$. The expression for Y_{eq} is given by [21]

$$Y_{eq} = \frac{45g}{4\pi^4} \frac{x^2 K_2(x)}{h_{eff}(m/x)} \quad (10)$$

where g is the number of internal degrees of freedom of the species under consideration (here $g = 1$), m is the mass and $K_n(x)$ is the modified bessel function of order n . From Eqs. (8) and (10), we obtain

$$\left(\frac{45}{\pi} G \right)^{-1/2} \frac{45g}{4\pi^4} \frac{K_2(x)}{h_{eff}(T)} g_*^{1/2} m \langle \sigma v \rangle \delta(\delta + 2) = \frac{K_1(x)}{K_2(x)} - \frac{1}{x} \frac{d \ln h_c(T)}{d \ln T} . \quad (11)$$

In the above equation, $h_c(T)$ is the contribution to $h_{eff}(T)$ from all species which are coupled to the universe at temperature T . Eq.(11) above is solved numerically in a self consistent manner in order to obtain the value of x_f (and hence the freeze out temperature $T_f (= m/x_f)$). In the present case we have taken the value of δ to be 1.5 [21]. Integrating Eq.(8) from $x = x_0 = m/T_0$ to $x = x_f = m/T_f$, where T_0 is the present photon temperature which is of the order of 10^{-14} GeV (~ 0), we obtain Y_0 (value of Y at $T = T_0$). Knowing Y_0 we can compute the relic density of the dark matter candidate (here S) from the relation [21],

$$\Omega h^2 = 2.755 \times 10^8 \frac{m}{\text{GeV}} Y_0 . \quad (12)$$

In the above $\Omega = \rho/\rho_c$ (ρ being the dark matter density and ρ_c is the critical density of the universe) and $h = \frac{H}{100 \text{ Km sec}^{-1} \text{ Mpc}^{-1}}$. Feynman diagrams in Fig. 1 represent the possible annihilation channels of S . The expressions for annihilation cross section $\langle\sigma v\rangle$ for the processes like $SS \rightarrow f\bar{f}, W^+W^-, ZZ, hh$ are given in refs.[22, 23] In this work we consider Higgs mass value

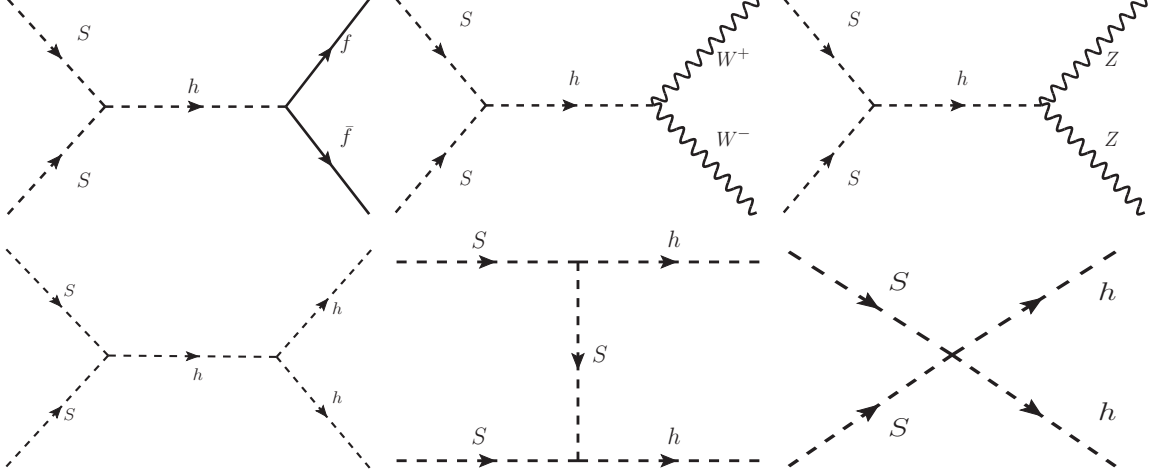


Figure 1: Lowest order Feynman diagrams of two S annihilate into a pair of fermion and anti-fermion, W^+W^- , ZZ and Higgs.

$m_h = 120 \text{ GeV}$. The variations of annihilation cross sections with scalar mass m_S are shown in Fig. 2 (Left Panel) for different values of δ_2 .

4 Calculational Procedure and Results

The relic density for scalar dark matter is obtained after an elaborate computation. We first calculate the freeze out temperature T_f for scalar dark matter with different values of coupling constant δ_2 and mass m_S . For this purpose we have solved Eq. (11) numerically. The values of the quantities $g_*^{1/2}$, $g_{eff}^{1/2}$ and h_{eff} for different T required for solving Eq.(11), are obtained from the figures (for the QCD phase transition temperature of 150 MeV) given in Refs. [21, 24]. In the Fig 2 (Right Panel), representative plots are the variations of T_f in the scalar dark matter mass range 5 GeV to 1 TeV for different values of δ_2 ($\delta_2 = 0.05, 0.1, 0.7$) and $m_h = 120 \text{ GeV}$ with the topmost plot is for the lowest value of δ_2 considered and the plots below are for other considered values of δ_2 in the increasing order. In general, the freeze out temperature T_f is approximately given by $T_f \sim m_S/20$. The plots for $T_f = m_S/20$ are also shown in Fig. 2 (Right Panel) (black dashed lines) for reference. The sudden dip in the values for T_f in Fig. 2 (Right Panel) around $m_S = 60 \text{ GeV}$ can be understood from the expression of $\langle\sigma v\rangle_{f\bar{f}}$ (given in refs. [22, 23]). At

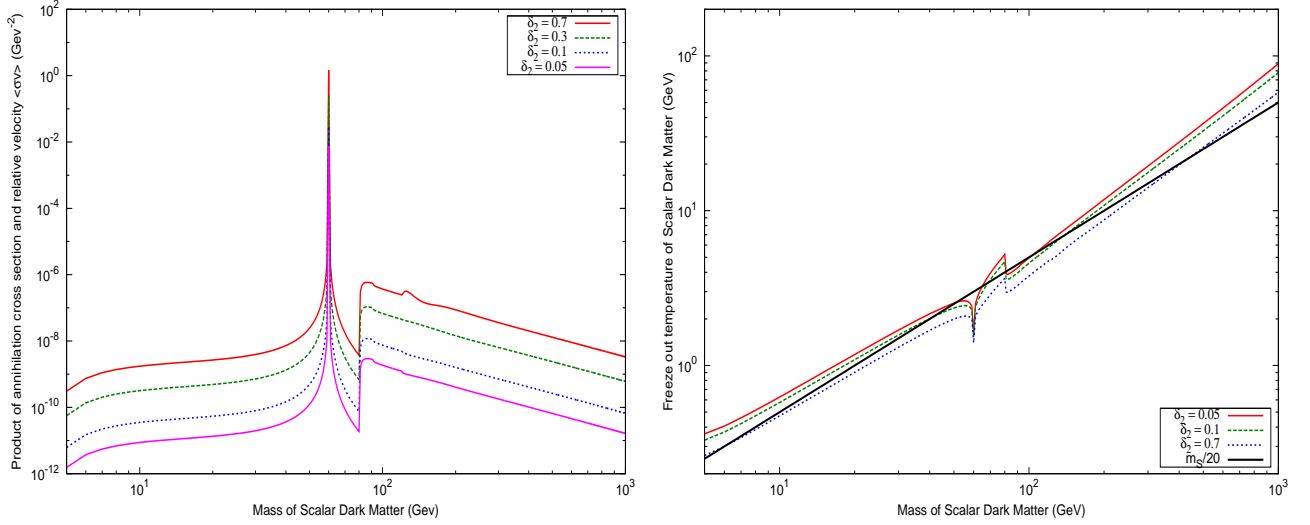


Figure 2: Left Panel : Variation of product of annihilation cross section and relative velocity $\langle\sigma v\rangle$ with the mass of scalar dark matter S for $\delta_2 = 0.7, 0.3, 0.1, 0.05$, Right Panel : Variation of freeze out temperature T_f with the mass for different values of $\delta_2 = 0.7, 0.1, 0.05$

this point there is a sudden rise in $\langle\sigma v\rangle$ (Fig. 2 (Left Panel)) and it is due to Higgs propagator appearing in the annihilation process ($SS \rightarrow f\bar{f}$). Using the values of freeze out temperatures (calculated from Eq. (11)) in Eq. (12) the relic densities of the scalar dark matter for different scalar dark matter masses and different values of δ_2 are computed. The results are shown in Fig. 3. In Fig. 3 the two parallel lines denote the WMAP limits on relic density of dark matter ($0.099 \leq \Omega h^2 \leq 0.123$). The different plots in Fig. 3 correspond to different values of δ_2 namely $\delta_2 = 0.05, 0.1, 0.3, 0.7$ respectively with the topmost one is for smallest value of δ_2 considered and the successive lower plots are for the other considered values of δ_2 in increasing order. We have seen from Fig. 2 (Left Panel) that initially the annihilation cross section of S increases with m_S ; then at $m_S \approx m_h/2$, $\langle\sigma v\rangle$ rises rapidly and after which it decreases with the increase of m_S . Again for $m_S \sim 81$ GeV, $\langle\sigma v\rangle$ suddenly increases upto nearly 2 orders of magnitudes from its value at $m_S \sim 80$ GeV and it is due to the fact that for $m_S > 80.4$ GeV the annihilation channel $SS \rightarrow W^+W^-$ becomes kinematically possible. Thereafter $\langle\sigma v\rangle$ starts decreasing with the increase of m_S . Since relic density is inversely proportional to $\langle\sigma v\rangle$ ⁴, the variation of relic density of dark matter particle S with m_S is just opposite to the variation $\langle\sigma v\rangle$ with m_S . This feature is reflected Fig. 3. Also since $\langle\sigma v\rangle$ is directly proportional to δ_2^2 and its higher powers, higher the value of δ_2 lower is the value of relic density (Fig. 3).

⁴ Physically we can say that $\langle\sigma v\rangle$ is directly proportional to probability of that process. So for higher $\langle\sigma v\rangle$ the probability of pair annihilation of S is high and hence density is low

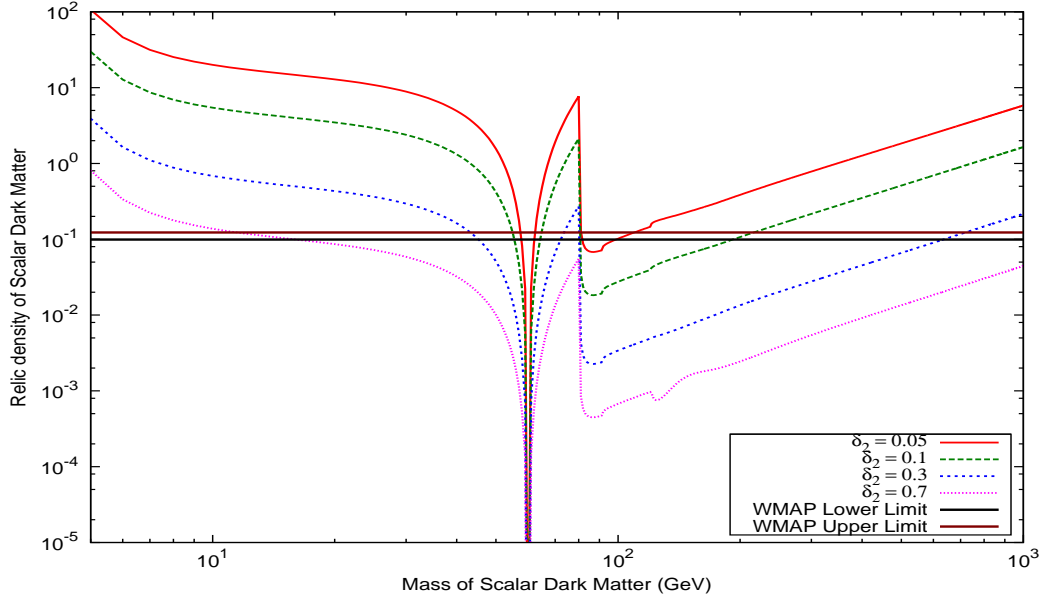


Figure 3: Variation of relic density Ωh^2 with the mass of scalar dark matter for Higgs mass 120 GeV

5 Constraining the model parameter δ_2

The model parameter δ_2 is a very important parameter for this present model because it appears in both the expressions of annihilation and scattering cross section of scalar dark matter S . The spin independent scattering cross section for scalar dark matter S is given later in Eq. (13). In this section we have constrained the parameter space $(m_S - \delta_2)$ by using WMAP limit on relic density of dark matter and the results of recent experiments like CoGeNT, DAMA, CDMS-II, XENON-10, XENON-100 and EDELWEISS-II. Similar to the previous discussions, here also we perform the calculations for Higgs mass $m_h = 120$ GeV with m_S in the range $5 \text{ GeV} \leq m_S \leq 1 \text{ TeV}$. The results obtained are shown in Fig. 4. We first use the WMAP limit ($0.099 \leq \Omega h^2 \leq 0.123$) on relic density of dark matter and using that limit we get the allowed values of m_S for each value of δ_2 (from Fig. 3). These results are shown in Fig. 4 using turquoise coloured contour. Thereafter we estimate the allowed values of δ_2 and m_S using the mass - cross section limits given by the experiments like CDMS-II, DAMA, CoGeNT, XENON-10, XENON-100, EDELWEISS-II and Eq. (13). In Fig. 4 the magenta coloured contour represent the allowed regions of scalar dark matter S obtained from CoGeNT data (2010). The overlap regions between these contours (magenta and Turquoise) are therefore satisfied by both WMAP and CoGeNT (2010) results. From the overlap region (Fig. 4) the range of m_S (in GeV) is found to be $7.7 \leq m_S \leq 11.15$ and the corresponding range of coupling δ_2 is obtained as $0.7 \leq \delta_2 \leq 0.95$.

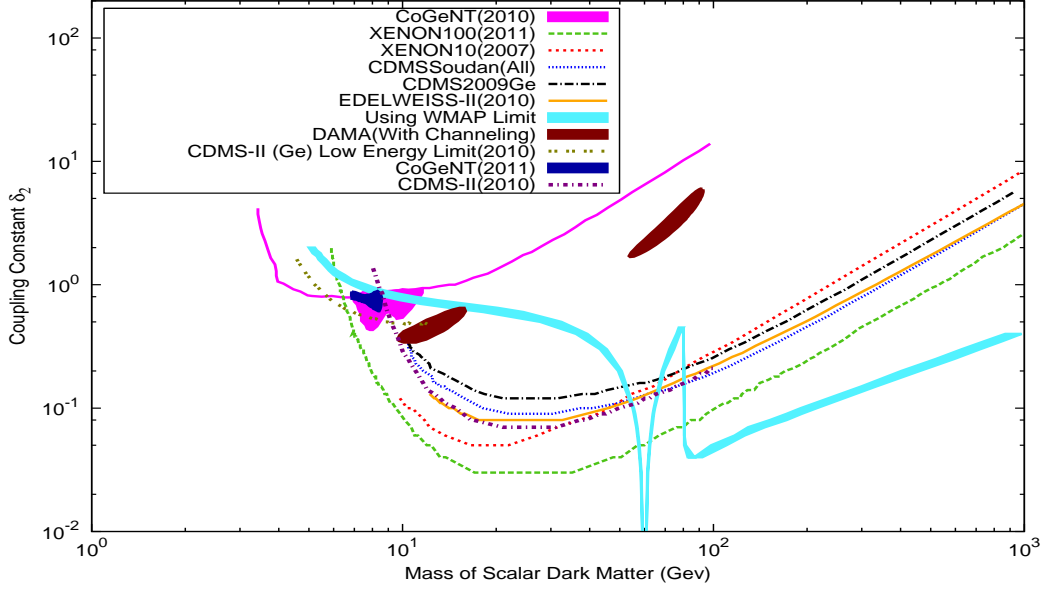


Figure 4: Constraining the parameter space ($m_S - \delta_2$) of scalar dark matter for Higgs mass 120 GeV (upper panel) by using WMAP limit and recent experimental results of CDMS-II, XENON-10, XENON-100, CoGeNT, DAMA, EDELWEISS-II.

These ranges therefore satisfy both WMAP and CoGeNT (2010) limits. The dark blue coloured contours indicate (Fig. 4) new bounds from CoGeNT data (2011) [19]. The common region between CoGeNT (2011) and WMAP lies in the range $8.0 \leq m_S \leq 8.53$ GeV, $0.8 \leq \delta_2 \leq 0.9$. This common intersection region is also well supported by CoGeNT (2010) and CDMS-II (2010) data [25] (purple dashed line).

Similar $m_S - \delta_2$ contours obtained from the DAMA experiment results (with channeling) are shown as maroon contours in Fig. 4. One sees that the small overlap regions between the two contours (turquoise and maroon) are restricted by the scalar mass (in GeV) range $14.8 \leq m_S \leq 15.9$. The corresponding values of δ_2 are found around 0.6. We remark in the passing that we have checked for other allowed regions in “dark matter mass $-\sigma_{\text{nucleon}}^{\text{scalar}}$ ” plane given by DAMA experiment but we have not obtained any overlap region such as described above. One of such regions (maroon coloured contour) is also shown in Fig. 4. The olive dashed line in Fig. 4 represent upper bounds that we have obtained from low energy analysis of the CDMS-II Germanium data [17]. But it has no intersection with WMAP satisfied region (turquoise coloured contour).

But unlike CoGeNT and DAMA, other experiments like XENON-10, XENON-100, CDMS-II, EDELWEISS-II do not provide a bounded allowed region in $m_S - \sigma_N$ plane (σ_N is the scattering cross section of dark matter and nucleon). Instead they provide upper bounds of scattering cross

section for a particular mass of dark matter. Consequently we also obtain upper bounds of δ_2 for a specific mass of S for those experiments. These results are also shown in Fig. 4. In Fig. 4 green dashed line represents the upper bound of δ_2 for XENON-100. CDMS-II results (CDMS 2009 Ge and CDMS Soudan (All) ⁵) are shown by black and blue dashed lines. XENON-10 and EDELWEISS-II results are represented by red dashed, orange solid line respectively. The WMAP results (turquoise plot in Fig. 4) intersect with the upper bounds obtained from XENON-10 results in $m_S - \delta_2$ plane are found to be at the values of $m_S = 53.5, \delta_2 = 0.12, m_S = 67.4, \delta_2 = 0.16$ and $m_S = 80.2, \delta_2 = 0.21$. Therefore the turquoise region below $(m_S = 53.5, \delta_2 = 0.12), (m_S = 67.4, \delta_2 = 0.16)$ and $(m_S = 80.2, \delta_2 = 0.21)$ is obeyed by both WMAP and XENON-10. Similarly the regions satisfied by both CDMS-II results (CDMS 2009 Ge, CDMS Soudan (All)) and WMAP are represented by the turquoise colour below intersection points $(m_S = 52.0, \delta_2 = 0.15), (m_S = 67.9, \delta_2 = 0.17), (m_S = 80.3, \delta_2 = 0.20)$ and $(m_S = 53.9, \delta_2 = 0.12), (m_S = 66.5, \delta_2 = 0.14), (m_S = 80.4, \delta_2 = 0.16)$ respectively as shown in the Fig. 4. Also the overlap regions of WMAP, XENON-100 and WMAP, EDELWEISS-II are below the following intersection points, can be read out from the Fig. 4 as $(m_S = 57.6, \delta_2 = 0.05), (m_S = 62.5, \delta_2 = 0.05), (m_S = 80.5, \delta_2 = 0.07)$ and $(m_S = 54.1, \delta_2 = 0.11), (m_S = 66.7, \delta_2 = 0.14), (m_S = 80.4, \delta_2 = 0.17)$. We have also found that for XENON-100 there is another intersection point with WMAP in the lower mass region around $m_S \sim 6.0$ GeV, $\delta_2 \sim 1.25$.

From the above analyses it appears that there are two distinct regions in the $m_S - \delta_2$ plane for scalar dark matter S which are allowed regions for both WMAP and recent experiments. The regions can be classified as follows.

- A lower mass region where we have found 3 mass ranges for scalar dark matter S . These ranges are given by $m_S \sim 6$ GeV ($\delta_2 \sim 1.25$), $7.7 \text{ GeV} \leq m_S \leq 11.15 \text{ GeV}$ ($0.7 \leq \delta_2 \leq 0.95$) and $14.8 \text{ GeV} \leq m_S \leq 15.9 \text{ GeV}$ ($\delta_2 \sim 0.6$). The corresponding ranges for coupling δ_2 which we have found are given within brackets. This lower mass domain is supported by WMAP and various ongoing dark matter direct detection experiments. In this case $m_S \sim 6$ GeV is supported by WMAP and XENON-100. Second and third mass ranges are obeyed by WMAP, CoGeNT (2010) data and WMAP, DAMA (with channeling) data respectively (Fig. 4).

But if we use more recent data of CoGeNT (CoGeNT (2011) data) then the second mass range of scalar dark matter S gets reduced to $8.0 \text{ GeV} \leq m_S \leq 8.53 \text{ GeV}$. The ranges for coupling δ_2 also reduced to $0.8 \leq \delta_2 \leq 0.9$. It is also seen from Fig. 4 that this region is supported by CDMS-II (2010) bounds. Other mass ranges are remain unchanged.

⁵Which are the results obtained by the CDMS-II collaboration from the combined analysis of full data set of Soudan.

- A higher mass region with the scalar dark matter mass range $\sim 52.5\text{GeV} \leq m_S \leq \sim 1000$ GeV, with the range of δ_2 found as $0.02 \leq \delta_2 \leq 0.4$ (Fig. 4). This mass region is satisfied by the allowed domains of WMAP, CDMS-II, EDELWEISS-II, XENON-10 and XENON-100.

Here we make some comments about the region of the parameter space (m_S vs δ_2) that is not satisfied by the results of direct detection experiments we have considered. In this region ($15\text{ GeV} < m_S < 52.5\text{ GeV}$) the values of δ_2 required to obtain current relic density (within WMAP limit) are such that the scattering cross sections obtained using these values for different dark matter masses do not satisfy the experimental limits given by different exclusion plots.

6 Formalism for the Calculations of Direct Detection Rates

In this section we estimate the differential direct detection rates and their annual variations for scalar dark matter S . For this purpose we have chosen ^{76}Ge and ^{131}Xe as a detector materials. The direct detection of dark matter by a terrestrial detector uses the principle of elastic scattering of dark matter particles off the detector nuclei and the energy of the recoil nucleus is measured. It is very difficult to measure the low recoil energy of nuclei accurately and hence a very low threshold and low background detector is required. In Fig. 5 we show the Feynman diagram for such elastic scattering process of scalar singlet S through Higgs exchange. The scalar singlet S - nucleon N elastic scattering ($SN \rightarrow SN$) cross section [26] is given by

$$\sigma_N^{\text{scalar}} = \frac{\delta_2^2 v^2 |\mathcal{A}_N|^2}{4\pi} \left(\frac{m_r^2}{M_S^2 M_h^4} \right), \quad (13)$$

where, $m_r(N, S) = M_N M_S / (M_N + M_S)$ is the reduced mass, \mathcal{A} is coupling between Higgs and nucleon N and its value is $\sim 340\text{ MeV}/V$ [26], with V being the VEV of Higgs boson. The scalar singlet - nucleus elastic scattering cross section is given by [26]

$$\sigma_{\text{nucleus}}^{\text{scalar}} = \frac{A^2 m_r^2(\text{nucleus}, S)}{m_r^2(\text{nucleon}, S)} \sigma_{\text{nucleon}}^{\text{scalar}}. \quad (14)$$

In the above A is the mass number of the nucleus. The differential detection rate of dark matter per unit detector mass is given by [27]

$$\begin{aligned} \frac{dR}{dE_R} &= \frac{\sigma_{\text{nucleus}}^{\text{scalar}} \rho_S}{4v_e m_S m_r^2} F^2(E_R) \\ &\times \left[\text{erf} \left(\frac{v_{\min} + v_e}{v_0} \right) - \text{erf} \left(\frac{v_{\min} - v_e}{v_0} \right) \right] \\ &= \frac{1}{T_1 T_2 T_3}, \end{aligned} \quad (15)$$

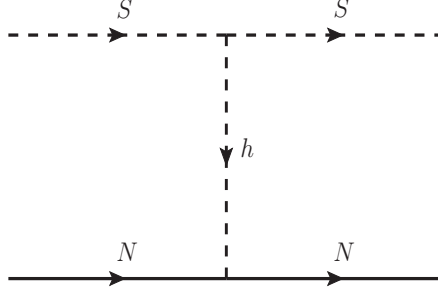


Figure 5: Feynman diagram for the elastic scattering between S and nucleon N via Higgs exchange.

where

$$T_1 = \frac{\sigma_{\text{nucleus}}^{\text{scalar}} \rho_S}{4v_e m_S m_r^2}, \quad T_2 = F^2(E_R),$$

$$T_3 = \left[\text{erf} \left(\frac{v_{\min} + v_e}{v_0} \right) - \text{erf} \left(\frac{v_{\min} - v_e}{v_0} \right) \right]. \quad (16)$$

Where v_e is the velocity of earth with respect to galactic frame of reference. And its expression is given by [27],

$$v_e = v_{\odot} + v_{\text{orb}} \cos \gamma \cos \left(\frac{2\pi(t - t_0)}{T} \right). \quad (17)$$

In the above expression t denotes any time of the year, $T = 1$ year is the time period of earth's motion around the sun, $v_{\text{orb}} = 30$ Km/sec is earth's orbital speed and $\gamma \simeq 60^\circ$ is the angle subtended by the ecliptic at the galactic plane. The solar velocity v_{\odot} is given by

$$v_{\odot} = v_0 + v_{\text{pec}}, \quad (18)$$

where v_0 is the circular speed of sun around the galactic centre taken to be 220 Km/sec and v_{pec} is the peculiar velocity with $v_{\text{pec}} = 12$ Km/sec. The periodicity in Eq. (17) causes an annual modulation of the event rates of dark matter in a terrestrial detector which serve as a definite signal of dark matter detection. In the Eq. 15 $F(E_R)$ is the nuclear form factor given by [28], ρ_S is the dark matter density in the solar neighbourhood, equal to 0.3 GeV/cm^3 for the rest of our calculations in this section. v_{\min} denotes the minimum velocity of dark matter required to produce a recoil energy E_R . The expression of v_{\min} is given by,

$$v_{\min} = \left(\frac{m_{\text{nucleus}} E_R}{2m_r^2} \right)^{1/2}. \quad (19)$$

The measured response of the detector by the scattering of dark matter off detector nucleus is in fact a fraction of the actual recoil energy. Thus, the actual recoil energy E_R is quenched by a factor q_X (different for different nucleus X) and we should express differential rate in Eq. (15) in terms of $E = q_X E_R$. Thus the differential detection rate (events/Kg/Day/keV) in terms of the observed recoil energy E for a monoatomic detector like Xe can be expressed as

$$\frac{\Delta R}{\Delta E}(E) = \int_{E/q_{\text{Xe}}}^{(E+\Delta E)/q_{\text{Xe}}} \frac{dR_{\text{Xe}}}{dE_R}(E_R) \frac{dE_R}{\Delta E} . \quad (20)$$

The total detection rate of dark matter is obtained by integrating Eq.(15) as

$$R = \int_{E_T}^{\infty} \frac{dR}{dE_R} dE_R , \quad (21)$$

where E_T is the threshold energy for a given detector material.

7 Direct Detection Rates for Scalar Dark Matter

In the present work, computations of direct detection rates are performed with $m_h = 120$ GeV, $\Delta E = 0.5$ keV and at a time $t = t_0$. As discussed earlier we have computed the direct detection rates and their annual variations for each of the detector materials namely ^{76}Ge , ^{131}Xe . The quenching factors for $^{76}\text{Ge} = 0.25$ [29], $^{131}\text{Xe} = 0.8$ [29], The differential detection rates and their annual variations can now be computed using Eqs. (15) - (21).

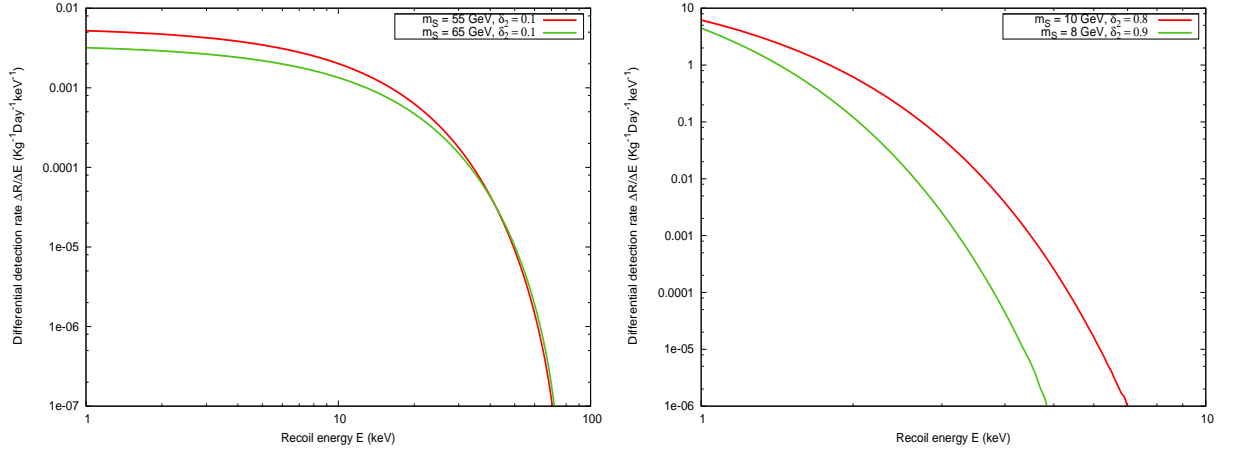


Figure 6: Variation of differential detection rates $\Delta R/\Delta E$ of scalar dark matter S with observed recoil energy E for monoatomic detectors Xe (left panel), Ge (right panel)

The variation of differential detection rates of scalar dark matter S with observed recoil energy E for mono atomic targets like Xe, Ge are shown in Fig. 6. In the left panel of Fig. 6,

we show the estimates of differential detection rates for different values of observed recoil energy E , with Xe as target material for $m_S = 55$ GeV (red solid line) and $m_S = 65$ GeV (green solid line). For both the cases the value of the coupling constant δ_2 is taken to be 0.1 (in agreement with the higher mass region described in section 5). Left panel of Fig. 6 shows that although the two plots corresponding to two scalar masses are distinguishable at lower recoil energies (≤ 11 GeV), at higher recoil energies they tend to coincide. In the right panel of Fig. 6 we show the direct detection rates results for the case of Ge. In this case, calculations are performed for two sets of $m_S - \delta_2$ values namely $(m_S = 10 \text{ GeV}, \delta_2 = 0.8)$, $(m_S = 8 \text{ GeV}, \delta_2 = 0.9)$. These values are chosen from the allowed lower mass domain discussed in section 5 (Fig. 4). It is seen from the right panel of Fig. 6 that the rates for the set $(m_S = 8 \text{ GeV}, \delta_2 = 0.9)$, represented by green solid line), falls off faster than those for the set $(m_S = 10 \text{ GeV}, \delta_2 = 0.8)$, represented by red solid line). The nature of $\Delta R/\Delta E$ for the case of Xe (left panel of Fig. 6) can be explained

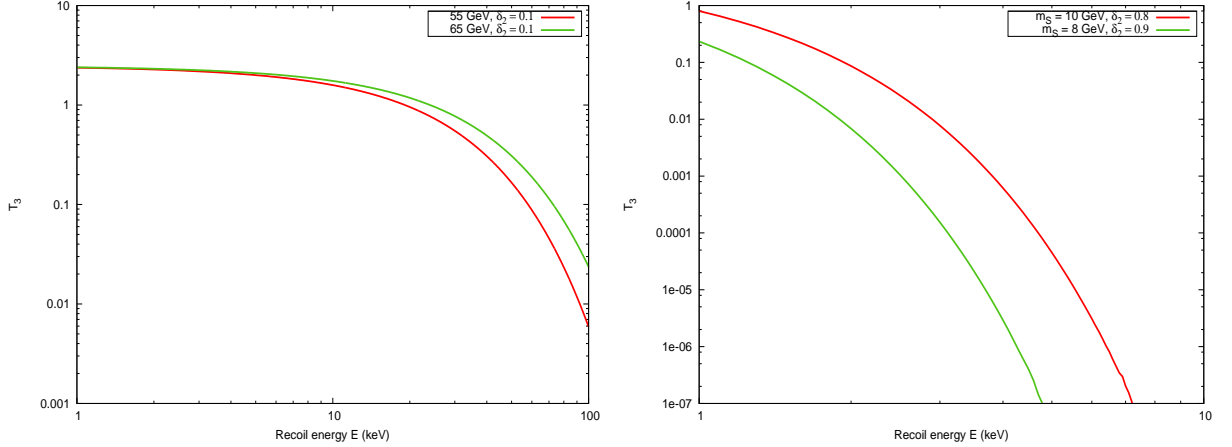


Figure 7: Left panel - Variation of T_3 with observed recoil energy E for Xe with $m_S = 55$ GeV (green solid line), 65 GeV (red solid line). Right panel - Same for Ge with $m_S = 10$ GeV (red solid line), 8 GeV (green solid line)

by examining the variation of T_3 (Eq. 16) with E . This is shown in left panel of Fig. 7. For low values of E and for high mass range of S ($m_S \gtrsim 55$ GeV), v_{min} (Eq. 19) $\ll v_e$ and hence T_3 is effectively independent of E . Therefore as E increases, the values of T_3 for $m_S = 65$ GeV becomes larger than those for $m_S = 55$ GeV. Also $\sigma_{nucleus}^{scalar}$ is inversely proportional to m_S and T_1 is directly proportional to $\sigma_{nucleus}^{scalar}$. Consequently T_1 is inversely proportional to m_S . Now the variation of $\Delta R/\Delta E$ with E is due to the combined effects of both T_1 and T_3 (Eq. (15)). This explains the nature of the plots for Xe in Fig. 6. In the case of Ge however, T_1 is nearly the same for both the masses considered. Consequently the variations of $\Delta R/\Delta E$ with E (Fig. 6 (right panel)) is dominated only by the nature of variations of T_3 with E . This variations are

shown in right panel of Fig. 7 which explains the nature of variations of $\Delta R/\Delta E$ with E for Ge.

The annual variations of total detection rates of WIMP is a crucial evidence for dark matter. This variation is caused by the periodic motion of earth around the sun in which the directionality of earth's motion changes over the year. Since the solar system moves towards the direction of Cygnus constellation, earth experiences a WIMP wind apparently coming from the direction of Cygnus. Due to the periodic motion of earth, the relative speed between earth and WIMP changes over the year. It becomes maximum when both the velocities of solar system and earth are in the same direction (on 2nd June) in which case the earth encounters maximum WIMP flux. The WIMP flux encountered by the earth is minimum when velocities of earth and sun are in opposite direction. Consequently, maximum events are expected on 2nd June of every year.

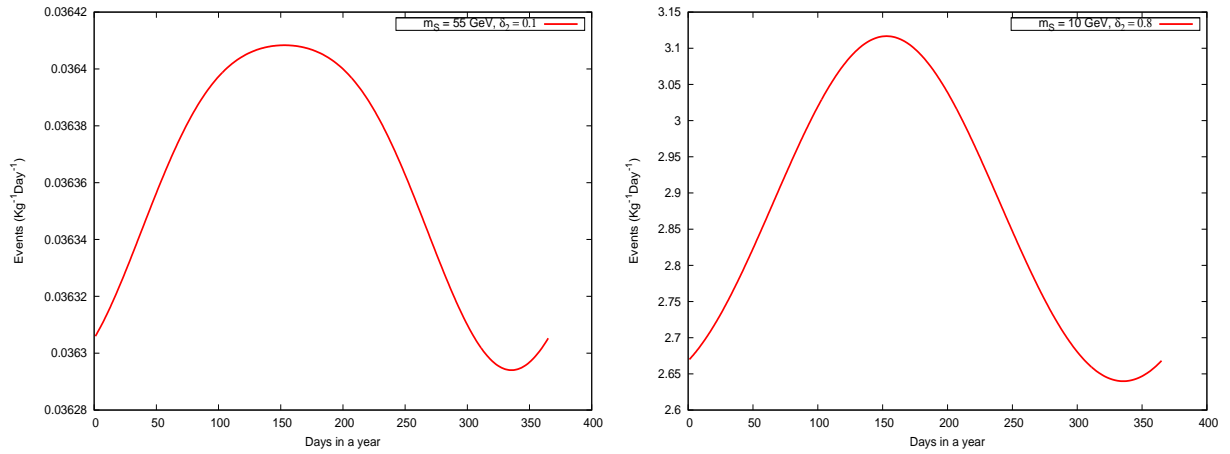


Figure 8: Left panel - Annual variation of total detection rates of scalar dark matter for Xe (mono atomic target) with $m_S = 55$ GeV, $\delta_2 = 0.1$. Right panel - Same for Ge with $m_S = 10$ GeV, $\delta_2 = 0.8$

In this work we compute the total detection rates at each day of a year, for the same detector materials namely Xe, Ge considering the scalar singlet as dark matter candidate. The results are then plotted with the days of year which show the annual variation of total detection rates. The calculations for Xe are performed for the set ($m_S = 55$ GeV, $\delta_2 = 0.1$) whereas for Ge, the set ($m_S = 10$ GeV, $\delta_2 = 0.8$). The results for Xe and Ge are shown in left and right panels of Fig. 8 respectively. All the plots in Figs. 8 show that the maximum expected events are at $t = 153$ (day) (corresponds on 2nd June).

8 Indirect Detection of Scalar Dark Matter

Another promising method for the detection of dark matter (WIMPs) is the observation of annihilation products of dark matter present in the galactic halo. In this section we will consider γ -rays coming from the dark matter annihilation in the galactic centre (GC).

Recently it has been reported that there is a 4.6σ (3.3σ) [30, 31] local (global) evidence of a monochromatic gamma-ray line with an energy $E_\gamma \approx 130$ GeV by the publicly available data [32] of Fermi Large Area Telescope (Fermi-LAT). This signal comes from two regions one of which is nearly at the centre of our galaxy ($-1^\circ, -0.7^\circ$), hereinafter referred to as the “central region” and another is located at $(-10^\circ, 0^\circ)$, called the “west region”. Both regions are extended within a circle of radius of 3° . It is suggested that this excess of gamma ray signal from galactic centre (GC) is not associated with the Fermi bubbles [31] and may result from dark matter annihilation into two monochromatic gamma-rays.

We have calculated the γ -rays flux due to 130 GeV scalar dark matter annihilation in the “central region” of our Milky way galaxy. The Feynman diagram for the process $SS \rightarrow \gamma\gamma$ is shown in Fig. 9. The expression of γ -ray flux due to dark matter annihilation in galactic halo

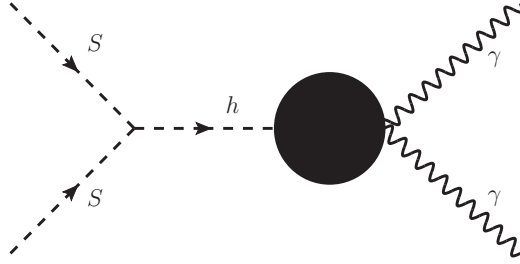


Figure 9: Feynman diagram for the process $SS \rightarrow \gamma\gamma$

is given by [33],

$$\frac{d\Phi_\gamma}{dE_\gamma} = \frac{1}{8\pi} \frac{\langle\sigma v\rangle_{SS\rightarrow\gamma\gamma}}{m_S^2} \frac{dN_\gamma}{dE_\gamma} r_\odot \rho_\odot^2 J, \quad (22)$$

where

$$J = \int db \int dl \int_{l.o.s} \frac{ds}{r_\odot} \cos b \left(\frac{\rho(r)}{\rho_\odot} \right)^2 \quad (23)$$

and

$$\frac{dN_\gamma}{dE_\gamma} = 2\delta(E - E_\gamma). \quad (24)$$

Mass of Scalar Dark Matter GeV	Coupling δ_2	Flux using Einasto Profile GeV cm ⁻² s ⁻¹ sr ⁻¹	Flux using NFW Profile GeV cm ⁻² s ⁻¹ sr ⁻¹	Flux using Isothermal Profile GeV cm ⁻² s ⁻¹ sr ⁻¹
130	0.06	1.971×10^{-7}	9.801×10^{-8}	4.048×10^{-9}

Table 1: γ -ray flux obtained from the annihilation channel $SS \rightarrow \gamma\gamma$, for three different dark matter halo profiles.

In the above, l and b are the galactic longitude and latitude respectively. We have performed l , b integration (in Eq. 23) over the “central region” of the our galaxy and the s integration (in Eq. 23) along the line of sight (l.o.s). Relation between r and s is given by

$$r = (s^2 + r_\odot^2 - 2sr_\odot \cos l \cos b)^{\frac{1}{2}}, \quad (25)$$

where $r_\odot = 8.5$ Kpc, the distance of the sun from the galactic centre and $\rho_\odot = 0.4$ GeV/cm³ is the dark matter halo density at the position of the solar system. The expression of the annihilation cross section $\langle\sigma v\rangle_{ss\rightarrow\gamma\gamma}$ (in Eq. 22) for the process shown in Fig. 9 is given in Ref. [34]. In this calculation we have taken three different dark matter halo profiles (available in literature) namely the Einasto profile [35], the NFW profile [36] and the Isothermal profile [37]. These halo profiles give the functional dependence of $\rho(r)$ with r . In the present calculation we have considered the value of the coupling $\delta_2 = 0.06$, which is allowed by WMAP and all recent ongoing dark matter direct detection experiments that have been considered in this work (Fig. 4, section 5). We have calculated the γ -ray fluxes for all the halo three profiles considered above and the results are shown in Table 1. The annihilation cross section $\langle\sigma v\rangle_{ss\rightarrow\gamma\gamma}$ is calculated to be 7.13×10^{-31} cm³/s for $\delta_2 = 0.06$. From Ref. [31], one sees that the γ -ray flux obtained from “central region” of our galaxy is in the range 4.0×10^{-5} to 7.5×10^{-5} (in GeV cm⁻²s⁻¹sr⁻¹) (95% CL) with best fit value, 5.6×10^{-5} GeV cm⁻²s⁻¹sr⁻¹. From Table 1 we see that in order to compare our results to those in Ref. [31] the annihilation cross section for the channel $SS \rightarrow \gamma\gamma$ in the present calculation must be enhanced by a factor of $\sim 3.0 \times 10^2$ (for the Einasto profile) and $\sim 5.7 \times 10^2$ (for the NFW profile) with respect to best fit value. As a result we have to increase coupling δ_2 from 0.06 to 1.03 (for the Einasto profile) and 1.43(for the NFW profile) respectively. From Fig. 4 it is seen that such a high value of δ_2 is not satisfied by either any direct detection experiments we have considered in this work or by the WMAP limits. Therefore we conclude that a 130 GeV dark matter in the present model can not explain the Fermi-LAT observed 130 GeV γ -ray line in the direction of the galactic centre unless the process is boosted (by introducing a boost factor [38]) either by astrophysical justifications and/or by other particle physics methods.

9 Summary and Conclusion

In the present work we consider a simplest extension of SM by introducing a real gauge singlet (singlet under $SU(2)_L \times U(1)_Y$) scalar S to SM which can only interact with SM particles via Higgs. For the stability of S , Z_2 symmetry is imposed in the theory. Thus S can be a viable candidate for cold dark matter. The scalar mass m_S and the coupling are the two parameters in the theory. We have calculated the freeze out temperature and relic density of this scalar dark matter candidate S by solving Boltzmann's equation and have constrained the $m_S - \delta_2$ parameter space by using WMAP limit on relic density of dark matter in the universe and the results of recent ongoing dark matter direct search experiments like CDMS-II, DAMA, CoGeNT, XENON-10, XENON-100. We find that if S is a dark matter candidate then its mass appears to be constrained within two regions. One is a lower mass region where m_S can vary from 6 GeV to 16 GeV with δ_2 lies in the limit $0.7 \leq \delta_2 \leq 1.25$ for $m_h = 120$ GeV. This region is supported by WMAP, CoGeNT and DAMA data. The other region is higher mass region with the ranges for m_S (in GeV) and δ_2 found out to be $52.5 \lesssim m_S \lesssim 1000$, $0.02 \leq \delta_2 \leq 0.4$ for the same Higgs mass. This region is also supported by the limits given by WMAP, CDMS-II, XENON-10, XENON-100, EDELWEISS-II experiments. We have calculated the possible differential direct detection rates and annual variations of total detection rates for scalar dark matter S in case of two detector materials namely Ge, Xe. For all these target materials we have found that differential detection rates decrease rapidly with the increase of observed recoil energy and they become vanishingly small for recoil energies beyond 10 keV for Ge with scalar mass $m_S = 10$ GeV. Whereas for Xe, the rates become vanishingly small for recoil energies beyond 80 keV when $m_S = 55$ GeV. We have also shown how the total rates vary over a year for these target materials. These annual variations of total detection rates, if found, will be one sure evidence for dark matter detection. Finally in the last section we have calculated the γ -ray flux for a 130 GeV scalar dark matter S and we have found that it is not possible to explain the Fermi-LAT observed excess γ -ray line by a 130 GeV scalar dark matter, unless a boost factor of order of 10^2 is introduced with the annihilation cross section of $SS \rightarrow \gamma\gamma$ channel.

Acknowledgments: A.B. thanks Debabrata Adak for some valuable discussions.

References

- [1] D. N. Spergel *et al.* [WMAP Collaboration], *Astrophys. J. Suppl.* **170**, 377 (2007); E. Komatsu *et al.* [WMAP Collaboration], *Astrophys. J. Suppl.* **180**, 330 (2009).
- [2] D. E. McLaughlin, arXiv:astro-ph/9812242.

- [3] E. L. Lokas and G. A. Mamon, Mon. Not. Roy. Astron. Soc. **343**, 401 (2003); [arXiv:astro-ph/0302461].
- [4] M. Bradac, Nucl. Phys. Proc. Suppl. **194**, 17 (2009)
- [5] V. Silveira and A. Zee, Phys. Lett. B **161**, 136 (1985).
- [6] M. C. Bento, O. Bertolami, R. Rosenfeld and L. Teodoro, Phys. Rev. D **62**, 041302 (2000); [arXiv:astro-ph/0003350], J. McDonald, Phys. Rev. Lett. **88** (2002) 091304; [arXiv:hep-ph/0106249], H. Davoudiasl, R. Kitano, T. Li and H. Murayama, Phys. Lett. B **609**, 117 (2005); [arXiv:hep-ph/0405097], D. O'Connell, M. J. Ramsey-Musolf, and M. B. Wise, Phys. Rev. D **75** (2007) 037701; [arXiv:hep-ph/0611014], V. Barger, P. Langacker, M. McCaskey, M. J. Ramsey-Musolf and G. Shaughnessy, Phys. Rev. D **77** (2008) 035005; arXiv:0706.4311[hep-ph], Carlos E. Yaguna, JCAP **0903** (2009) 003 arXiv:0810.4267[hep-ph], X. G. He, T. Li, X. Q. Li, J. Tandean and H. C. Tsai, Phys. Rev. D **79** (2009) 023521; arXiv:0811.0658[hep-ph], X.G. He, T. Li, X.Q. Li, J. Tandean, and H.C. Tsai, Phys.Lett. B **688**, 332 (2010); arXiv:0912.4722[hep-ph], X.G. He, S.Y. Ho, J. Tandean, and H.C. Tsai, Phys.Rev.D **82**, 035016 (2010); arXiv:1004.3464[hep-ph], A. Bandyopadhyay, S. Chakraborty, A. Ghosal, D. Majumdar, JHEP **1011** (2010) 065; arXiv:1003.0809[hep-ph], M. Asano and R. Kitano, Phys. Rev. D **81** (2010) 054506; arXiv:1001.0486[hep-ph].
- [7] M. H. G. Tytgat; arXiv:1012.0576[hep-ph].
- [8] S. Andreas, T. Hambye, M. H. G. Tytgat, JCAP **0810** (2008) 034; arXiv:0808.0255[hep-ph].
- [9] R. Bernabei *et al.* [The DAMA collaboration], Eur. Phys. J. C **56**, 333 (2008); AIP Conf. Proc. **698**, 328 (2004); Int. J. Mod. Phys. D **13**, 2127 (2004).
- [10] C. E. Aalseth *et al.* [The CoGeNT collaboration]; arXiv:1002.4703 [astro-ph.CO].
- [11] Z. Ahmed *et al.* [The CDMS-II Collaboration]. arXiv:0912.3592[astro-ph.CO].
- [12] S. Andreas, C. Arina, T. Hambye, F. S. Ling and M. H. G. Tytgat, Phys. Rev. D **82** (2010) 043522; arXiv:1003.2595[hep-ph].
- [13] E. Aprile *et al* [The XENON 100 collaboration], arXiv:1104.2549v2[astro-ph.CO].
- [14] A. Liam Fitzpatrick, D. Hooper, K. M. Zurek; arXiv:1003.0014[hep-ph].
- [15] A. A. Abdo et al., Astrophys. J. **712**, 147 (2010); arXiv:1001.4531[astro-ph.CO].

- [16] C. Arina and M. H. G. Tytgat, JCAP **1101** (2011) 011; arXiv:1007.2765[astro-ph.CO], C. Balazs, N. Sahu and A. Mazumdar, JCAP **0907**, 039 (2009); arXiv:0905.4302 [hep-ph], K. Kohri, J. McDonald and N. Sahu, Phys. Rev. D **81**, 023530 (2010); arXiv:0905.1312 [hep-ph], C. Arina, F. -X. Josse-Michaux and N. Sahu, Phys. Rev. D **82**, 015005 (2010); arXiv:1004.3953 [hep-ph].
- [17] Z. Ahmed *et al.* [The CDMS-II Collaboration], PRL **106**, 131302 (2011); arXiv:1011.2482[astro-ph.CO].
- [18] J. Angle *et al* [The XENON 10 Collaboration], Phys. Rev. Lett. **100**, 021303 (2008); [arXiv:astro-ph/0706.0039], E. Aprile and T. Doke, Rev. Mod. Phys. **82**, 2053 (2010).
- [19] C. E. Aalseth *et al.* [The CoGeNT collaboration], PRL **107**, 141301 (2011); arXiv:1106.0650[astro-ph.CO].
- [20] E. Armengaud *et al* [The EDELWEISS Collaboration], arXiv:1103.4070v2[astro-ph.CO]
- [21] P. Gondolo and G. Gelmini, Nucl. Phys. B **360**, 145 (1991).
- [22] J. McDonald, Phys. Rev. D **50**, 3637 (1994); arXiv:hep-ph/0702143.
- [23] W-L. Guo and Y-L. Wu, JHEP **1010** (2010) 083; arXiv:1006.2518[hep-ph].
- [24] M. Srednicki, R. Watkins and K. A. Olive, Nucl. Phys. B **310**, 693 (1988).
- [25] M. Felizardo *et al.* [The SIMPLE Collaboration]; arXiv:1106.3014[astro-ph.CO].
- [26] C. P. Burgess, M. Pospelov and T. ter Veldhuis, Nucl. Phys. B **619**, 709 (2001); arXiv:hep-ph/0011335.
- [27] G. Jungman, M. Kamionkowski and K. Griest, Phys. Rept. **267**, 195 (1996); arXiv:hep-ph/9506380.
- [28] J. Engel, Phys. Lett. B **264**, 114 (1991).
- [29] A. Bottino, V. de Alfaro, N. Fornengo, G. Mignola, S. Scopel, Astropart. Phys. **2**, 77 (1994).
- [30] C. Weniger, JCAP **1208**, 007 (2012); arXiv:1204.2797 [hep-ph],
- [31] E. Tempel, A. Hektor and M. Raidal, arXiv:1205.1045 [hep-ph].
- [32] W. B. Atwood *et al.* [LAT Collaboration], Astrophys. J. **697**, 1071 (2009); arXiv:0902.1089 [astro-ph.IM].

- [33] M. Ackermann *et al.* [LAT Collaboration], arXiv:1205.2739 [astro-ph.HE].
 - [34] S. Profumo, L. Ubaldi and C. Wainwright, Phys. Rev. D **82**, 123514 (2010); arXiv:1009.5377 [hep-ph].
 - [35] J. Einasto, Trudy Inst. Astrofiz. Alma-Ata **5** (1965) 87, J. F. Navarro *et al.*, Mon. Not. Roy. Astron. Soc. **349**, 1039 (2004); astro-ph/0311231.
 - [36] J. F. Navarro, C. S. Frenk and S. D. M. White, Astrophys. J. **490**, 493 (1997); astro-ph/9611107.
 - [37] J. N. Bahcall and R. M. Soneira, Astrophys. J. Suppl. **44**, 73 (1980).
 - [38] A. Sommerfeld, Annalen der Physik **403**, 257 (1931), N. Arkani-Hamed, D. P. Finkbeiner, T. R. Slatyer and N. Weiner, Phys. Rev. D **79**, 015014 (2009); arXiv:0810.0713 [hep-ph], Q. -H. Cao, I. Low and G. Shaughnessy, Phys. Lett. B **691**, 73 (2010); arXiv:0912.4510 [hep-ph].
-